A Distinct Metabolite Profile Correlates with Neurodegenerative Conditions and the Severity of Congenital Hydrocephalus

Authors: García-Bonilla M, García-Martín ML, Muñoz-Hernández MC, Domínguez-Pinos D, Martínez-León MI, Peñalver A, Castilla L, Alonso FJ, Márquez J, Shumilov K, Hidalgo-Sánchez R, Gutiérrez A, Páez-González P, Jiménez AJ.

Abstract

In congenital hydrocephalus, cerebrospinal fluid accumulation is associated with increased intracranial pressure (ICP), ischemia/hypoxia, metabolic impairment, neuronal damage, and astrocytic reaction. The aim of this study was to identify whether a metabolite profile revealing tissue responses according to the severity of hydrocephalus can be detected. The hyh mutant mouse used for this study exhibits 2 different forms of hydrocephalus, severe and moderate. In a comprehensive investigation into the 2 progressions of hydrocephalus, mice with severe hydrocephalus were found to have higher ICP and astrocytic reaction. Several metabolites from the mouse brain cortex were analyzed with 1H high-resolution magic angle spinning nuclear magnetic resonance (1H HR-MAS NMR) spectroscopy. A differential profile for metabolites including glutamate and glutamine was found to correlate with the severity of hydrocephalus and can be explained due to differential astrocytic reactions, neurodegenerative conditions, and the presence of ischemia. The glutamate transporter EAAT2 and the metabolite taurine were found to be key histopathological markers of affected parenchymata. In conclusion, a differential metabolite profile can be detected according to the severity of hydrocephalus and associated ICP and therefore can be used to monitor the efficacy of experimental therapies.

Key Words: Astrocytic reaction, Congenital hydrocephalus, Glutamate, Glutamine, Intracranial pressure, Magnetic resonance spec-roscopy, Taurine.

INTRODUCTION

Hydrocephalus is a distension of the ventricles based on increased cerebrospinal fluid (CSF) volume, which can be caused by obstruction of CSF flow (noncommunicating hydrocephalus) or increased production/decreased reabsorption (communicating

hydrocephalus). Congenital hydrocephalus is one of the most common disorders treated by pediatric neurosurgeons, with an estimated incidence of 4–6 per 10 000 births (1, 2). Although surgically treated cases survive with the present-day standard of care (3), the complexity of the disease makes it difficult to obtain reliable data on outcomes. The pathophysiology of hydrocephalus is complex and leads to alterations of the normal physiology, biochemistry and ultrastructure of the brain (4). Several studies have attempted to identify CSF biomarkers that might be useful for diagnosis and therapy (5, 6).

In hydrocephalic infants and animal models with experimental hydrocephalus, hypoperfusion of the blood flow in various regions of the cerebral cortex, including the white matter, has been recorded (7). Energy metabolism is impaired in hydrocephalus, leaving the cerebral tissue especially vulnerable to hypoxic and ischemic lesions (4). Periventricular axons and myelin are the primary targets of injury in hydrocephalus, revealing pathogenic similarities with traumatic and ischemic white matter injury (8–10). In human cases of hydrocephalus, neurons and myelin have been reported to be affected by and probably related to the presence of brain edema, anoxic ischemic conditions, oxidative stress and glutamate excitotoxicity (11). In animal models, pathological changes in neurons are not dramatic, and they are probably secondary to axonal damage (8, 12–16). There is not an extensive amount of neuronal death either (14, 17). However, astrocytic reactions in the ventricular walls are common (18–22).

The hyh mutant mouse presents a mutation in the Napa gene, which encodes aSNAP, a protein that is implicated in vesicular trafficking (23). The trigger and etiology of the obstructive hydrocephalus developed in the hyh mouse have been described in previous articles (22, 24, 25), proving the model to be an excellent animal model for infant hydrocephalus. Although the hyh mice present the same genetic background, they exhibit 2 forms of the disease that differ in their severity and have been named rapidly and slowly progressive hydrocephalus (RPH and SPH, respectively) (26). Whereas most hyh mice with RPH die during the first month of life, those with SPH are able to survive for more than a year (27).

The differences in the 2 forms of development of hydrocephalus can be explained on the basis of (i) the range of time during which the obliteration at the caudal end of the cerebral aqueduct occurs (25) and (ii) the presence of spontaneous ventriculostomies that could drain the excess of CSF (26).

The present study has been designed as a comprehensive investigation into the 2 forms of development of hydrocephalus developed by the hyh mice to uncover the following: First, whether both forms of hydrocephalus evolution are associated with differences in intracranial pressure (ICP); and, second, whether differences in ICP are associated with specific neurodegenerative conditions and with a specific set of metabolites that can serve as indicators for monitoring therapies.

Two regions of the brain cortex, the neocortex and hippocampus, were studied because they are differentially affected during hydrocephalus progression (22, 27). In the neocortex, edema and damage in the periventricular white matter were especially pronounced. The metabolic profile was analyzed and compared using 1H high-resolution magic angle spinning nuclear magnetic resonance (1H HR-MAS NMR) spectroscopy in tissue biopsies from these brain regions.

Our results showed, first, the existence of a direct correlation between ICP and the severity of hydrocephalus and, second, the existence of significant differences in the metabolite spectra according to the severity of hydrocephalus. The metabolite taurine and the glutamate transporter EAAT2 have been shown to be good histopathological indicators of the degree to which the brain parenchymata are affected in hydrocephalus. Thus, the methodology used in the present study to detect significant metabolites for the severity of hydrocephalus can be extrapolated to studies in humans.

MATERIALS AND METHODS

Experimental Animals

Mutant hyh mice (hydrocephalus with hop gait, B6C3Fe-a/a-hyh/J strain) and their wild-type (wt) littermate controls were used for the study. The mice were originally obtained from The Jackson Laboratory (Bar Harbor, ME) and bred by the Animal Experimentation Service of the University of Malaga. All the animals were housed in the same room with a 12-hour:12-hour light/dark cycle at 22 C and with standard food and water available ad libitum. Experimental procedures were approved by the Institutional Animal Care and Use Committee of the University of Malaga (CEUMA). Accordingly, in addition to the design of the experiments, the housing, handling, care and processing of the animals were conducted in accordance with European and Spanish laws (RD53/2013 and 2010/63UE) and followed the ARRIVE guidelines (28). Wt and mutant hyh mice were identified by clinical inspection and genotyping (29). Hyh mice with RPH and SPH were identified by phenotype according to the criteria described by Batiz et al (26), including motor activity (Supplementary Data, Video V1 of a normal and an hyh mouse with RPH and SPH at the ages used in this study), body weight (Fig. 1A), macrocephaly (Fig. 1B–D), and expansion of the lateral ventricles. Wt and hyh mice, females and males in equal proportions in each group, were killed by cervical dislocation at 20 days of age to quickly obtain the samples after death for 1H HR-MAS NMR analysis or under anesthesia with Dolethal (sodium pentobarbital; Vetoquinol, Lure, France; intraperitoneal administration, 0.2 mg/g bodyweight) for immunocytochemistry/immunofluorescence processing. For the measurement of ICP, the animals were anesthetized with 3% sevoflurane in 1 L/minute of oxygen. Sampling for 1H HR-MAS NMR analysis was conducted at midday 61 hour.
ICP recordings were carried out in the afternoon. Performing functional behavioral analyses, such as negative geotaxis and rotarod tests, was disregarded in the hyh mice due to their abnormal motor coordination/balance and the gait of the rearlegs (30) (Supplementary Data, Video V1 of 20-day-old hyh mice; Supplementary Data, Videos V2 and V3 of normal and hyh mice at 6 days of age).

Intracranial Pressure

Wt (n = 10) and hyh mice (RPH, n ¼ 13; SPH n ¼ 4) were placed under sevoflurane anesthesia in an adapted stereotaxic instrument. In the wt mice, a 1-mm-diameter hole was drilled in the right parietal bone above the lateral ventricle using the coordinates of 1.1 mm lateral and 0.1 mm caudal to bregma. In the hyh mice, the hole was drilled in the bone covering the distinguishably enlarged lateral ventricle. A length of noncompliant tubing was filled with artificial CSF and connected to a disposable pressure transducer (MLT0670, Power Lab System, AD Instruments, Oxford, UK) interfaced with a recording system (PowerLab System, FE117, AD Instruments) using LabChart (AD Instruments). The end of the tubing contained a needle. In wt mice, ICP was measured in the lateral ventricle by introducing the needle according to the method described by Oshio et al (31). ICP was measured at high resolution, and arterial pulsations could be detected. For the hyh mice, because of the thinning of the brain cortex, the measurements were obtained at the moment when the needle punctured a strained point on the lysed bone and reached the visible lumen of the lateral ventricle.

Measurement of Cerebral Hemisphere Sizes

After ICP measurement, mice were anesthetized with sevoflurane and killed by cervical dislocation. Then, the brains were quickly dissected and immersed in Bouin's fixative for 4 days at room temperature. After being washed with 0.1 M phosphate-buffered saline (PBS) at pH 7.4, the brains were imaged under a stereomicroscope. An estimation of the cerebral hemisphere size was obtained by multiplying the dimensions of the micrographs taken from the dorsal and lateral views. Finally, the brains were embedded in paraffin and used for immunohistochemical analyses.

Quantification of Metabolites

H HR-MAS NMR spectroscopy was used to obtain the metabolic profiles of the dissected samples. Mice used for ICP pressure procedures were discarded for quantification metabolites analysis to avoid the influence of anesthesia and surgical procedures in this quantification. The hippocampus and neocortex of wt (n ¼ 20) and hyh (RPH, n ¼ 24; SPH, n ¼ 12) mice were quickly removed under cold conditions, frozen using dry ice and stored at 84 C. Frozen samples were cut to fit into 30-mL disposable cylindrical inserts. The inserts were placed into an HR-MAS zirconium rotor (4-mm OD) and transferred to the HR-MAS probe, which was cooled to 4 C. The HR-MAS spectra were acquired on a 600-MHz Bruker Avance Spectrometer (Bruker BioSpin, Ettlingen, Germany) at 4 C at a 5-kHz spinning rate. For absolute metabolite quantification, an artificial reference signal was added into each NMR spectrum using the ERETIC2 method (electronic reference to access in vivo concentrations) implemented in TopSpin 3.1 (Bruker BioSpin), which is based on the PULCON principle (pulse length-based concentration determination) that originates from the principle of reciprocity (32, 33).

This artificial peak was used as an internal reference for the concentration determination with LCModel (34), as described by Righi et al (35).

Immunohistochemistry/Immunofluorescence

Paraffin sections (10-mm thick) of the brains from the mice (wt, n ¼ 5; RPH, n ¼ 11; SPH, n ¼ 8) used for the ICP measurement were used for quantitative immunohistochemistry. After heat-induced antigen retrieval in 50 mM citrate buffer at pH 6.0, cell markers were labeled with specific antibodies (Table 1) and then with the corresponding biotinylated secondary antibodies (Dako, Glostrup, Denmark), ExtrAvidin-peroxidase (Sigma, St. Louis, MO), and 3,30 -diaminobenzidine tetrahydrochloride ([DAB], Sigma) as an electron donor for histochemical detection. Immunofluorescence was also developed in paraffin sections according to the protocol described below.
For tissue immunolocalization of metabolites and enzymes, wt and hyh (wt, n ¼ 7; RPH, n ¼ 12; SPH, n ¼ 3) mice were transcardially perfused with 4% paraformaldehyde diluted in 0.1 M phosphate buffer at pH 7.4. The fixed brains were removed and postfixed in the same solution for 24 hours at 4 C. Then, the brains were sectioned with a vibratome (80-lm-thick sections) or were cryoprotected in 30% sucrose to obtain 60-lm-thick frozen sections. Each type of section was tested to obtain the best labeling. The thickness of sections was selected trying to preserve the best integrity during staining procedures. When antibodies worked well in Bouin-fixed/paraffin sections, they were preferred for analysis. Analyses were done and shown according to the best of these conditions.
The vibratome and frozen sections were processed with a freefloating section-staining protocol for immunohistochemistry/immunofluorescence (Table 1). The immunohistochemistry followed a protocol similar to the one described above for paraffin sections, and ammonium nickel sulfate was added to intensify the DAB reaction. For immunofluorescence, secondary antibodies conjugated with Alexa Fluor 488 or Alexa Fluor 568 (Thermo Fisher, Waltham, MA) were applied. Nuclear staining was performed with 40 , 6-diamidino-2-phenylindole ([DAPI], Molecular Probes, Eugene, OR). Immunofluorescence images were obtained with Leica SP5 and SP8 laser confocal microscopes (Leica, Wetzlar, Germany). For each experiment, the images were acquired at a time with the same settings. The images were used to create the figures, and only minimal changes in brightness and contrast were applied equally for all the experimental groups.
The antibodies for immunostaining were diluted in PBS containing 0.05% Triton X-100 (Sigma) and 0.01% sodium azide. Primary antibody incubations were performed for 18 hours at 22 C or for 72 hours at 4 C. Secondary antibody and ExtrAvidin incubations were performed for 1 hour at 22 C. For negative controls, the primary antibodies were omitted

Image Analysis

Histological quantifications were carried out in paraffin sections that had been immunostained at the same time and under the same conditions. Micrographs were obtained by scanning with a VS120 microscope (Olympus, Tokyo, Japan) with an UPLSAPO20x/0.75 objective and were processed with ImageJ software (NIH). The densities (cells/area) of astrocytes and neurons were calculated in 6 fields per section (10-mm thickness) per animal in the parietal cortex. The fields for astrocyte quantification were of different sizes in order to exclude the gray matter and the particular astrocytic reaction that covered the ependyma-denuded surface (see Roales-Bujan et al [36]). Optical density of immunofluorescence was calculated from confocal images taken from frozen sections (wt, n ¼ 5; RPH, n ¼ 4; SPH, n ¼ 4) by an SP8 Leica microscope using a hybrid sensor (HyD). The quantification tool in LAS-AF Lite (Leica Application Suite, Leica) was used

Statistics

Statistical analyses were performed using KaleidaGraph (Synergy Software, Reading, PA), SPSS (IBM, Armonk, NY), and Statgraphics Centurion XVII (Statpoint Technologies, Warrenton, VA). For characterization of the groups, the differences of both ICP records and data obtained with immunohistochemistry/immunofluorescence for some markers (glutamate and EAAT2) were quite pronounced. For these experiments, 4–13 animals were used for appropriate statistical analyses.
For spectroscopy, the required sample size was estimated according to standard deviations or significance with a minimum of 30 degrees of freedom. Animals were numbered in random order without indication of group. For spectrometry and micrograph quantification, data collection and analysis were blinded by using different researchers and masking of the samples. Since we did not see noticeable differences between male and female mice in the experiments, we used both for the analyses. All values are reported in the figures as the mean-
6 SEM. The Wilcoxon-Mann-Whitney test and Student t-test were applied for hypothesis testing in situations requiring nonparametric and parametric analyses, respectively. When the F probability from the Student t-test was <0.05, the variance was considered unequal. $p < 0.05$ based on both tests was considered to indicate statistical significance. For correlations, Spearman's rank-order coefficients were calculated.
A multivariate analysis was carried out to identify the differential metabolite profiles that represent each group of mice. Metabolites following normal distributions were selected for this analysis. Two discriminant functions were obtained (Di ¼ a0 þ a1X1 þ . . . þ anXn) on the basis of the quantified metabolites. These functions allowed the classification of the mice into the 3 different groups and the identification of the most influential and reliable metabolites. Using the probabilities of belonging to the groups, data that were obtained from the multivariate analysis, the receiver operating characteristics (ROC) curve was calculated to identify the cutoff levels and the optimal combination of specificity and sensitivity. Because the levels of aspartate, glutamine and glutamate did not follow a normal distribution, logistic regression (LR) was performed to test these metabolites as possible classifiers for differentiating between

the mouse groups. In this case, the prediction function is exponential, the relationship between the variables Xn and P is nonlinear, and the parameters Bn were estimated using the LR algorithm. As in the multivariate analysis, larger Bn values indicated larger impact of the variables Xn.

$$P[v=3] = \exp(B_0 + B_1X_1 + \ldots + B_nX_n)/(1 + \exp(B_0 + B_1X_1 + \ldots + B_nX_n))$$

$$Z = B_0 + B_1X_1 + B_2X_2 + \ldots + B_nX_n$$

TABLE 1. Antibodies

Antibody	Source	Reference	Type	Use	Dilution
EAAT2	Santa Cruz Biotechnology	Sc-365634	Mouse monoclonal	FR	1:100
GFAP	Sigma	G-A-5	Mouse monoclonal	PF, VB, FR	1:1000
Glutamate	Sigma	G6642	Rabbit polyclonal	VB, FR	1:4000
Glutathione peroxidase	Abcam	ab108427	Rabbit monoclonal	PF, VB, FR	1:150
Glutamine synthetase	Abcam	ab49873	Rabbit polyclonal	PF, VB, FR	1:5000
Glutathione synthetase	GeneTex	GTX63666	Rabbit monoclonal	PF, VB, FR	1:100
Kidney-type glutaminase (KGA)	*	*	Rabbit polyclonal	VB, FR	1:500
NeuN	Merck Millipore	MAB377 Clone A60	Mouse monoclonal	VB, FR	1:500
Olig2	R&D Systems	AF2418	Goat polyclonal	VB, FR	1:1000
Taurine	Merck Millipore	AB5022	Rabbit polyclonal	VB, FR	1:100

Abbreviations: FR, frozen section; PF, paraffin section; VB, vibratome section. Sources: Abcam, Cambridge, UK; GeneTex, Irvine, CA; Merck Millipore, Darmstadt, Germany; R&D Systems, Minneapolis, MN; Santa Cruz Biotechnology, Dallas, TX; Sigma, St. Louis, MO.
*Obtained in the Canceromics Laboratory, Department of Molecular Biology and Biochemistry, University of Malaga (48).

RESULTS

Cases with Severe Hydrocephalus Exhibit Higher ICP

Hydrocephalic animals were grouped according to whether they exhibited RPH or SPH, following the criteria that had been previously described by Batiz et al (26). As examples, body weight (Fig. 1A) and hemisphere size (Fig. 1B–D) are shown. Previous studies with H-Tx rats (36) and kaolin-induced hydrocephalic rats (21) have shown that high ICP could be responsible for both the development of ventriculomegaly and cortical mantle thinning in such animal models. For this reason, ICP was recorded to test whether differences between hyh mice with RPH and SPH were present. Mice with severe hydrocephalus showed higher ICP than mice with moderate hydrocephalus (Fig. 1E, F). Interestingly, there were no significant differences between mice with SPH and wt mice (Fig. 1E, F).

The Intensity of the Astrocyte Reaction Is Increased in Severe Hydrocephalus

In the H-Tx rat and in rats with experimentally induced hydrocephalus, previous studies have established a relationship between ICP and the periventricular astrocytic reaction, where the astrocyte population decreases or improves after shunting and therefore with ICP reduction (37, 38). Differences in the intensity of the periventricular astrocytic reaction between cases with RPH and SPH were studied to see if a relationship with differences in ICP existed. To measure the intensity of the astrocytic reaction, GFAP-immunolabeled reactive astrocytes (density, cells/area) were quantified in the periventricular white matter (Fig. 1G–I). The particular astrocytic reaction that generated a periventricular barrier as described previously (39) was excluded from the analysis. The composition and cellular structure of this barrier made it impossible to accurately quantify individual cells (Fig. 1G, H). Therefore, the analysis was selectively performed in the periventricular white matter beneath the astrocyte barrier. The results showed a higher density of reactive astrocytes in the periventricular white matter in mice with RPH than in those with SPH (Fig. 1I).

Differences in Neuronal Densities in Specific Layers of the Neocortex Are Associated with the Severity of Hydrocephalus

The differences in the cortical thickness during development in hyh mice with RPH and SPH have been previously described (22). In the present study, such differences were evident in each of the groups of mice at the ages studied (Supplementary Data Fig. S1), and mice with RPH exhibited a remarkable reduction in thickness compared with that of mice with SPH. To determine whether these differences in thickness could be related to a loss of neurons, the density of NeuN positive cells (neurons/area) was quantified in the different neocortical cell layers. Layers 2–3 of the parietal cortex of mice with RPH presented higher neuronal densities compared with the same region in the parietal cortex of the controls (Fig. 2A–D). However, no significant differences were found in neuronal density in layer 5 among the 3 groups of mice (Fig. 2A–D).

A Specific Spectroscopic Metabolite Profile Can Be Detected According to the Severity of Hydrocephalus

For the study with 1H HR-MAS NMR spectroscopy, metabolites were selected according to in vivo MR spectroscopy in the human clinic (Supplementary Data Fig. S2). Metabolites that did not show significant differences between the study groups (acetate, alanine, glucose, glycerophosphocholine, isoleucine, and lactate; results not shown) were excluded from further analyses.
On the other hand, several metabolites showed significant differences between the study groups, displaying 3 major trends in the neocortex. The first trend comprised metabolites whose levels were increased in mice exhibiting severe hydrocephalus (RPH) compared with levels in normal mice and mice exhibiting moderate hydrocephalus (SPH). These metabolites were creatine, glutamine, taurine, N-acetyl-aspartate and threonine (Fig. 3A–D, H). A second trend consisted of

metabolites with higher levels in mice exhibiting RPH than in mice with SPH or normal mice. These metabolites were aspartate, N-acetyl-aspartyl-glutamate, glutamate, glutathione and phosphatidylethanolamine (Fig. 3E–G, J). Finally, a third trend consisted of some metabolites with higher levels in normal mice than in mice with RPH or SPH. These metabolites were inositol, GABA and total choline (Fig. 3K–M).
Importantly, in contrast to what was detected in the neocortex, levels of most of the metabolites in the hippocampus did not follow any of these trends (Fig. 3A–N).

Metabolite Profiles in Mice with Severe Hydrocephalus Are Highly Correlated

Correlations in the metabolic trends per animal were analyzed. Mice with RPH presented higher correlation coefficients among the metabolites than those in normal mice and mice with SPH (Supplementary Data Fig. S3). All of the correlations were stronger in the neocortex than those in the hippocampus (Supplementary Data Fig. S3).
The multivariate analysis was run using only the variables that showed significant differences between the mice with RPH and SPH and were normally distributed. This was the case for creatine, N-acetyl-aspartate, taurine and threonine.
With their metabolite profiles, the coefficients of the discriminant functions were obtained (Table 2), and a predictive classification of the mice was made (Table 3). The results showed that 62.5%, 75%, and 63.6% of the RPH, SPH, and wt mice, respectively, were classified in the correct groups (Table 3). The score plot based on the results of the multivariate analysis showed good separation with function 1 between mice with RPH and the other 2 groups (see the centroids in Fig. 4). With the multivariate analysis, the probabilities of belonging to each group were obtained and used by a ROC analysis. ROC comparison curves revealed statistically significant discriminations between the wt mice and mice with RPH, and mice with RPH and SPH, but not between wt mice and mice with SPH (Table 4).
To improve the classification process including the metabolites that did not follow a normal distribution, LR was carried out. All metabolites were tested, and the combination of aspartate, creatine, glutamate, glutamine, N-acetyl-aspartate, taurine and threonine showed the highest predictive score and the best percentage of correctly classified mouse groups (86.1% RPH vs SPH; 94.1% SPH vs wt; and 78.3% RPH vs wt). The results of the LR analysis showed that glutamate was the metabolite with the highest significantly predictive score that allows correct discrimination between the 3 groups of mice (Table 5). In addition, glutamine was also a good discriminator between wt mice and mice with SPH.
A study was carried out in brain sections to detect the presence of metabolites that were found to be significant in the spectroscopy analysis. When needed to complement the study, related enzymes or transporters were used as histopathological markers as described below.

Glutamate and Glutamine

In accordance with the spectroscopy results, immunostaining for glutamate showed significant differences in the neocortex between mice with RPH and SPH (Supplementary Data Fig. S4). In the neocortex of normal and hyh mice, glutamate was detected in normal and reactive astrocytes (Fig. 5A–E). Antibodies developed against the glutaminase (GLS) enzyme (EC 3.5.1.2; K-type mitochondrial glutaminase isoenzyme, KGA) (40), which convert glutamine into glutamate, labeled neurons in normal (Fig. 5F, G) and hydrocephalic mice (Fig. 5H, I). In hyh mice, KGA was also immunodetected in periventricular reactive astrocytes that were present in the white matter (Fig. 5I). In addition, immunolabeling for the glutamate transporter EAAT2 also showed differences between the groups of mice (Fig. 5J–M). The immunoreaction for EAAT2 was stronger in mice with RPH and present in astrocytes (Fig. 5K).

Immunodetection of Glutathione-Related Enzymes

Two enzymes related to glutathione, namely, glutathione synthetase and glutathione peroxidase, that use glutathione for reduction of peroxides were immunodetected in tissue sections. Both enzymes were found to be present in the neurons of wt and hyh mice (Supplementary Data Fig. S5). In the hyh mice, both enzymes were also immunodetected in periventricular reactive astrocytes (Supplementary Data Fig. S5).

Periventricular Neural Cells Express High Levels of Taurine in Mice with Severe Hydrocephalus

In the neocortex of normal mice, taurine was immunolocalized in neurons, astrocytes and ependymocytes (Fig. 6A–C). Immunolabeling with antitaurine antibodies revealed strong reactions in cells located in the most severely affected neocortical periventricular areas of mice exhibiting RPH (Fig. 6D, E) but not in mice with SPH (Fig. 6F, G). These cells in mice with RPH were identified as neurons, oligodendrocytes and astrocytes (Fig. 6E, H–J).

DISCUSSION

The present research was performed in a mutant animal model with congenital obstructive hydrocephalus exhibiting 2 different progressions: Severe hydrocephalus (RPH), a devastating phenotype; and moderate hydrocephalus (SPH), a form compatible with life (26).
Here, we have found a differential profile of metabolites between mice presenting high

ICP, those that exhibit RPH compared with those animals with ICP similar to normal mice, those that exhibit SPH. The differences are associated with responses in energy metabolism, neuron-astrocyte metabolic coupling, and neuroprotection. The higher astrocytic reaction present in the neocortex of mice with RPH and elevated ICP appears to be triggered by cortical stretching and compression, myelin degeneration and cell death, and hypoxic/ischemic conditions (41) and can be in part responsible for the metabolite profile as will be discussed below.

Two types of animal models have previously been used for the analysis of metabolites in hydrocephalus, where evidence has been given for a reduction in energy metabolism, membrane synthesis, neurotransmitters, and amino acids (42–47). One model is adult rats with induced hydrocephalus after injection of kaolin in the cisterna magna and thus acquired obstructive hydrocephalus. Alternatively, the H-Tx rat with congenital hydrocephalus is comparable to the hyh mouse, and both resemble human infantile hydrocephalus. Unlike the hyh mouse with severe hydrocephalus, in the H-Tx rat, levels of creatine, N-acetyl-aspartate, taurine, glutamine and glutamate were found to be reduced (42). The differences between the results from hyh mice and other models indicate that several variables, including the severity of ventriculomegaly, ICP and the rate of progression of ventricular dilatation, severely hamper the comparisons (46). The interest in the hyh mice underlie in their differential degree of hydrocephalus development linked to the differences in ICP. In the hyh mice, their differential metabolite profile probably reveals responses in the metabolism of astrocytes and neurons that can be related to ICP and ischemia.

In the neocortex of hyh mice with RPH compared with that of normal mice and mice with SPH, the profile of the metabolites creatine, threonine, glycine, glutamate, and aspartate could be an indicator of differential neurodegenerative conditions or metabolic tissue responses. Thus, these differential metabolic profiles could be associated with the effect of ventriculomegaly and high ICP, with oxygen deprivation due to high ICP. Energetic metabolism of neurons and astrocytes in these conditions can be implied in this differential profile.

In contrast, in the hippocampus of hyh mice with RPH, which would be similarly subjected to high ICP, the tendency was significant only for creatine. The contrast between the results obtained in the neocortex and the hippocampus could represent more intense cellular responses and damage, consistent with the higher myelin damage, edema, astrocytic reaction, and neurodegeneration present in the neocortex (22).

Creatine and Threonine

Creatine has been considered a marker for energy dependent system cells, and its levels tend to be low in diseases associated with low metabolism (48). In the hyh mouse with RPH, high levels of creatine can be related to a neuroprotective effect against anoxic and ischemic cell damage. The creatine/phosphocreatine system can

compensate to some extent for the lack of oxygen or glucose and is related to the energy store in the brain (49). Thus, phosphocreatine allows ATP synthesis in the absence of oxygen and glucose, as can occur in anoxia/ischemia (50). Threonine dehydrogenase in mitochondria gives rise to glycine and acetyl-CoA using threonine, thus contributing to energy production in the tricarboxylic acid cycle (51).

Glutamate and Glutamine

The energetic metabolism of astrocytes has been shown to be affected in experimental hydrocephalus (52). Under the ischemic conditions of severe hydrocephalus, astrocytes can be responsible for the differential levels of some metabolites, including glutamate and glutamine.

Glutamate and glutamine were the 2 metabolites that had a greater impact on the predictive function used in the analysis, allowing the discrimination between the 3 groups of animals. The higher levels of glutamate in the hyh mouse with severe hydrocephalus can be explained on the basis of altered energy metabolism or the coupled metabolism of astrocytes with neurons. Glutamate can be responsible for an excitotoxic and oxidant environment. The immature brain is vulnerable to the impairment of astrocyte and neuron metabolism by oxidative stress, including the regulation of glutamate levels (53).

Glutamate can act as an excitatory neurotransmitter and must be maintained in the correct extracellular concentrations to avoid its excitotoxic effects (54), which are related to neuronal death in ischemia, hypoglycemia, and trauma (55). Most of the glutamate is located in neurons, but glutamate dehydrogenase is mainly present in astrocytes (56), contributing to the tricarboxylic acid cycle and energy production (57). In a different pathway, aspartate aminotransferase, allows for the conversion of glutamate into the tricarboxylic acid cycle intermediate a-ketoglutarate (57). On the other hand, the presence of high levels of glutamate and glutamine could have different implications for the metabolic coupling between astrocytes and neurons. Glutamate can be reabsorbed by glial cells, including astrocytes, and can continue to many different endpoints (58). Thus, astrocytic glutamate transporters are essential for maintaining extracellular glutamate concentrations below toxic levels (59, 60). The astroglial glutamate transporter EAAT2 has been considered the main protector against excitotoxicity. In chronic ischemia, EAAT2 expression levels have been described to be increased in the white matter (61). The higher levels of EAAT2 detected in hyh mice with severe hydrocephalus support a tissue reaction related to the levels of glutamate. Thus, it is also possible for neurons to react to a high level of glutamate in hydrocephalus. Glutamate can be effectively converted to glutamine by the enzyme glutamine synthetase in astrocytes. Glutamine can be released by astrocytes and taken up by neurons in order to obtain glutamate using glutaminase. This metabolic coupling through the activity of glutamine synthetase and glutaminase, both present in reactive astrocytes, can underlie in the differences in the levels of both metabolites found here. The stronger astrocytic reaction in hyh mice with RPH can explain the higher levels of

glutamine, and the lower levels of glutamate found in the neocortex in hyh mice with SPH would indicate a less excitotoxic environment. Evidence in human infants with hydrocephalus (62) and in the hyh mouse regarding elevation in the levels of glutamine suggests that, in congenital hydrocephalus, there is an alteration in the glutamate/glutamine metabolism of astrocytes and neurons.

Glutamate and glycine, 2 metabolites found in higher concentrations in the neocortex of hyh mice with RPH, are the preferred extracellular amino acid precursors for glutathione synthesis in astrocytes, which is catalyzed by glutathione synthetase (63). The high cellular glutathione content and the strong capacity of astrocytes for glutathione-dependent detoxification processes help to protect not only these cells but also their neighbors against the toxic potential of oxidants and toxins. Furthermore, astrocytes supply 2 essential precursors, glutamine and glutamylcysteine, for glutathione synthesis in neighboring neurons (64). The presence of glutathione synthetase found in the reactive astrocytes in hyh mice can also explain the higher levels of glutathione detected in mice with severe hydrocephalus.

TABLE 4. ROC Analysis of the Discrimination Between the Different Groups

	Probability (0-1)	Cut-off level	Sensitivity (0-1)	Specificity (0-1)	AUC	p value*
RPH vs SPH	RPH	0.447	0.792	0.647	0.761	0.001*
	SPH	0.610	0.917	0.727	0.822	0.001*
SPH vs wt	SPH	0.509	0.750	0.864	0.818	0.02
	wt	0.490	0.484	0.75	0.818	0.002
RPH vs wt	RPH	0.354	0.833	0.773	0.862	<0.0001*
	wt	0.536	0.864	0.750	0.862	<0.0001*

The probability of belonging to each group (0 = group 1; 1 = group 2) obtained from the multivariate analysis was used to obtain the optimal threshold with the ROC analysis. *Abbreviations*: AUC, area under the curve; RPH, rapidly progressive hydrocephalus; SPH, slowly progressive hydrocephalus; wt, wild-type. p value refers to comparison with an AUC of 0.5.

TABLE 5. Logistic Regression Analysis of Metabolite Levels Between Groups of Mice

Metabolite	*B*	Standard Error	Wald	df	p Value*	e^B	Lower	Upper
RPH vs SPH								
Asp	2.395	2.241	1.143	1	0.285	10.971	0.136	885.884
Cre	–0.383	1.151	0.111	1	0.739	0.682	0.071	6.501
Gln	–0.246	1.175	0.044	1	0.834	0.782	0.078	7.826
Glu	1.419	0.713	3.965	1	0.046*	4.132	1.022	16.700
NAA	–1.845	1.285	2.063	1	0.151	0.158	0.013	1.959
Thr	2.899	3.265	0.788	1	0.375	18.155	0.030	10911.716
Tau	–1.033	0.643	2.586	1	0.108	0.356	0.101	1.254
SPH vs wt								
Asp	3.679	2.047	3.230	1	0.072	39.592	0.716	2187.799
Cre	–0.501	1.631	0.094	1	0.759	0.606	0.025	14.826
Gln	–4.624	2.132	4.706	1	0.030*	0.010	0.000	0.640
Glu	3.152	1.599	3.889	1	0.049*	23.389	1.019	536.619
NAA	–2.328	1.784	1.704	1	0.192	0.097	0.003	3.214
Thr	–7.199	3.774	3.639	1	0.056	0.001	0.000	1.219
Tau	0.781	0.702	1.235	1	0.267	2.183	0.551	8.649
RPH vs wt								
Asp	2.767	1.959	1.995	1	0.158	15.909	0.342	739.487
Cre	–1.216	0.980	1.539	1	0.215	0.296	0.043	2.024
Gln	–1.195	1.048	1.300	1	0.254	0.303	0.039	2.360
Glu	1.161	0.565	4.220	1	0.040*	3.193	1.055	9.669
NAA	–0.348	1.061	0.108	1	0.743	0.706	0.088	5.647
Thr	0.098	2.468	0.002	1	0.968	1.103	0.009	139.034
Tau	–0.296	0.422	0.493	1	0.483	0.743	0.325	1.701

For each metabolite (variable), the *B* equation coefficient, standard error, Wald-test statistics, degrees of freedom (*df*), p value, exponential of *B*, and the lower and upper confident intervals is shown. The logistic regression analysis discriminates significant metabolites for mice with rapidly progressive hydrocephalus (RPH), slowly progressive hydrocephalus (SPH) and normal mice (wt, wild-type).

*p value significant. *Abbreviations*: Asp, aspartate; Cre, creatine; Gln, glutamine; Glu, Glutamate; NNA, N-actetyl-aspartate; Thr, threonine; Tau, taurine.

Other Metabolites

N-acetyl-aspartate levels are typically used as a marker of neuronal density or viability (65). N-acetyl-aspartate and N-acetyl-aspartyl-glutamate are synthesized in neurons and can be exported to oligodendrocytes in order to obtain acetyl-CoA for myelin production (66). Furthermore, N-acetyl-aspartyl-glutamate is converted to N-acetyl-aspartate and glutamate by carboxypeptidases located on the extracellular surface of astrocytes (67). We detected higher levels of N-acetyl-aspartyl-glutamate and glutamate in the neocortex of hyh mice with RPH compared with those in mice with SPH. The detected levels of N-acetyl-aspartyl-glutamate can be correlated with the trends of neuronal densities (NeuN-positive cells) found in the hyh and wt mice. The higher density of NeuN-positive neurons in mice with RPH can be related with compression of the cortical tissue due to high ICP (compare layers 2–3 in Figure 2B0 and C0 showed with the same magnifications).

However, the levels of N-acetyl-aspartate could also be related to myelin turnover, mitochondrial energy metabolism from glutamate, or osmoregulation (65).

Phosphatidylethanolamine is one of the main phospholipids in plasma membranes and subcellular organelles (68).

The high levels of phosphatidylethanolamine found in the neocortex of the more severely affected hyh mice could represent myelin degradation/turnover (69). In

addition, phosphatidylethanolamine can be a substrate for phospholipases activated by glutamate, which is released in ischemia (70).
Myo-inositol is a cellular osmolyte that has also been considered a marker for glial content in brain tissue. It has been reported to be elevated in pathological states with prominent glial activation. Myo-inositol is one of the main osmolytes in the brain; it can be taken up by astrocytes in response to surrounding hyperosmolarity and can be released during hypo-osmolarity (71, 72). However, in the neocortex and hippocampus of hyh mice with RPH, as reported in rats with kaolin-induced hydrocephalus (44), the levels of myoinositol are lower despite the presence of extensive astroglial reactions.

Taurine as a Histopathological Marker of Tissue Damage in Hydrocephalus

Taurine, an organic osmolyte, is an antioxidant involved in cell volume regulation and in cytoprotective suppression of glutamate-induced toxicity and apoptosis (73, 74). An increased concentration of taurine has been described as particularly effective in mitigating ischemic or anoxic tissue damage (75). The high levels of taurine detected with 1H HR-MAS NMR spectroscopy in the neocortex and the hippocampus of mice with RPH and high ICP can be related with some of these proposed roles. In the hyh mice with RPH, the immunolabeling of taurine in neurons, astrocytes and oligodendrocytes in the more damaged periventricular regions suggests taurine as a good histopathological indicator of tissue damage or response

Conclusions, Applicability to Humans and Limitations of the Study

It has been possible to find that in hyh mice exhibiting different degrees of hydrocephalus severity and ICP, disease-dependent cellular responses can be monitored by the presence of particular metabolite profiles. The metabolism of neurons and astrocytes appears to be affected probably due to chronic ischemic and neurodegenerative conditions associated with high ICP. In addition, taurine and EAAT2 have been found to be reliable histopathological markers for the severity of hydrocephalus in such conditions. 1H HR-MAS NMR spectroscopy can be considered a useful tool for evaluation in ex vivo samples of experimental therapies in hydrocephalus, where in vivo NMR spectroscopy would not have been possible due to the voxel size required, as in the case of the hyh mice. Obviously, HR-MAS spectroscopy cannot be used as a diagnostic tool in humans with tissue biopsies that are not justified. However, due to the small size of the different brain areas in the mouse brain, this technology has allowed us to investigate the brain metabolic profile regionally. The present study has revealed differences between the neocortex and hippocampus, and it is important to consider the different degrees to which different brain areas are affected. It would be useful to translate the present findings to clinical diagnoses using in vivo NMR

spectroscopy instead of HR-MAS for the following metabolites: Lactate, alanine, acetate, N-acetyl-aspartate, N-acetyl-aspartyl-glutamate, glutamate, glutamine, creatine, total choline, myo-inositol, taurine and glycine. In particular, the metabolites glutamine, glutamate, and taurine can give valuable information in the neocortex. In addition, the translation of HR-MAS NMR for the diagnosis and monitoring in humans could be possible using CSF samples. Thus, this study provides an opportunity to consider NMR spectroscopy as a useful tool for monitoring hydrocephalus development in human cases.

ACKNOWLEDGMENTS

The authors wish to thank David Navas from the Microscopy Service of the University of Malaga (Spain) for his valuable technical support and all the staff of the Animal Experimentation Service of the University of Malaga (Spain) for their support during the experiments.

REFERENCES

1. Garne E, Loane M, Addor MC, et al. Congenital hydrocephalus – prevalence, prenatal diagnosis and outcome of pregnancy in four European regions. Eur J Paediatr Neurol 2010;14:150–5
2. Jeng S, Gupta N, Wrensch M, et al. Prevalence of congenital hydrocephalus in California, 1991–2000. Pediatr Neurol 2011;45:67–71
3. Vinchon M, Rekate H, Kulkarni AV. Pediatric hydrocephalus outcomes: A review. Fluids Barriers CNS 2012;9:18
4. da Silva MC. Pathophysiology of hydrocephalus. In: Cinalli G, SainteRose C, Maixner WJ, eds. Pediatric Hydrocephalus. Milano: Springer Milan 2005:65–77
5. Naureen I, Waheed KAI, Rathore AW, et al. Fingerprint changes in CSF composition associated with different aetiologies in human neonatal hydrocephalus: Glial proteins associated with cell damage and loss. Fluids Barriers CNS 2013;10:34
6. Limbrick DD, Baksh B, Morgan CD, et al. Cerebrospinal fluid biomarkers of infantile congenital hydrocephalus. PLoS One 2017;12:e0172353
7. Shirane R, Sato S, Sato K, et al. Cerebral blood flow and oxygen metabolism in infants with hydrocephalus. Childs Nerv Syst ChNS 1992;8:118–23
8. Del Bigio MR. Cellular damage and prevention in childhood hydrocephalus. Brain Pathol 2004;14:317–24
9. Del Bigio MR, da Silva MC, Drake JM, et al. Acute and chronic cerebral white matter damage in neonatal hydrocephalus. Can J Neurol Sci 1994;21:299–305
10. Khan OH, Enno TL, Del Bigio MR. Brain damage in neonatal rats following kaolin induction of hydrocephalus. Exp Neurol 2006;200:311–20
11. Castejon OJ. Submicroscopic pathology of human and experimental hydrocephalic cerebral cortex. Folia Neuropathol 2010;48:159–74

12. McAllister JP, Maugans TA, Shah MV, et al. Neuronal effects of experimentally induced hydrocephalus in newborn rats. J Neurosurg 1985;63:776–83
13. Wright LC, McAllister JP, Katz SD, et al. Cytological and cytoarchitectural changes in the feline cerebral cortex during experimental infantile hydrocephalus. Pediatr Neurosurg 1990–1991;16:139–55
14. Del Bigio MR, Zhang YW. Cell death, axonal damage, and cell birth in the immature rat brain following induction of hydrocephalus. Exp Neurol 1998;154:157–69
15. Ding Y, McAllister JP, Yao B, et al. Axonal damage associated with enlargement of ventricles during hydrocephalus: A silver impregnation study. Neurol Res 2001;23:581–7
16. Harris NG, McAllister JP, Conaughty JM, et al. The effect of inherited hydrocephalus and shunt treatment on cortical pyramidal cell dendrites in the infant H-Tx rat. Exp Neurol 1996;141:269–79
17. Jones HC, Bucknall RM, Harris NG. The cerebral cortex in congenital hydrocephalus in the H-Tx rat: A quantitative light microscopy study. Acta Neuropathol 1991;82:217–24
18. Sival DA, Guerra M, den Dunnen WFA, et al. Neuroependymal denudation is in progress in full-term human foetal spina bifida aperta. Brain Pathol 2011;21:163–79
19. Domınguez-Pinos MD, Paez P, Jimenez AJ, et al. Ependymal denudation and alterations of the subventricular zone occur in human fetuses with a moderate communicating hydrocephalus. J Neuropathol Exp Neurol 2005;64:595–604
20. Deren KE, Packer M, Forsyth J, et al. Reactive astrocytosis, microgliosis and inflammation in rats with neonatal hydrocephalus. Exp Neurol 2010; 226:110–9
21. Olopade FE, Shokunbi MT, Siren A-L. The relationship between ventricular dilatation, neuropathological and neurobehavioural changes in hydrocephalic rats. Fluids Barriers CNS 2012;9:19
22. Paez P, Batiz L-F, Roales-Bujan R, et al. Patterned neuropathologic events occurring in hyh congenital hydrocephalic mutant mice. J Neuropathol Exp Neurol 2007;66:1082–92
23. Chae TH, Kim S, Marz KE, et al. The hyh mutation uncovers roles for alpha Snap in apical protein localization and control of neural cell fate. Nat Genet 2004;36:264–70
24. Jimenez AJ, Tome M, Paez P, et al. A programmed ependymal denudation precedes congenital hydrocephalus in the hyh mutant mouse. J Neuropathol Exp Neurol 2001;60:1105–19
25. Wagner C, Batiz LF, Rodrıguez S, et al. Cellular mechanisms involved in the stenosis and obliteration of the cerebral aqueduct of hyh mutant
mice developing congenital hydrocephalus. J Neuropathol Exp Neurol 2003;62:1019–40
26. Batiz LF, Paez P, Jimenez AJ, et al. Heterogeneous expression of hydrocephalic phenotype in the hyh mice carrying a point mutation in alpha-SNAP. Neurobiol Dis 2006;23:152–68
27. Jimenez AJ, Rodrıguez-Perez L-M, Domınguez-Pinos MD, et al. Increased levels of tumour necrosis factor alpha (TNFa) but not transforming growth factor-beta 1 (TGFb1) are associated with the severity of congenital hydrocephalus in the hyh mouse: TNFa in the aetiology of congenital hydrocephalus. Neuropathol Appl Neurobiol 2014;40:911–32
28. Kilkenny C, Browne WJ, Cuthill IC, et al. Improving bioscience research reporting: The ARRIVE guidelines for reporting animal research. PLoS Biol 2010;8:e1000412
29. Batiz LF, Roales-Bujan R, Rodrıguez-Perez LM, et al. A simple PCR-based genotyping

method for M105I mutation of alpha-SNAP enhances the study of early pathological changes in hyh phenotype. Mol Cell Probes 2009;23:281–90
30. Bronson RT, Lane PW. Hydrocephalus with hop gait (hyh): A new mutation on chromosome 7 in the mouse. Brain Res Dev Brain Res 1990;54:131–6
31. Oshio K, Watanabe H, Song Y, et al. Reduced cerebrospinal fluid production and intracranial pressure in mice lacking choroid plexus water channel Aquaporin-1. FASEB J 2005;19:76–8
32. Monakhova YB, Kohl-Himmelseher M, Kuballa T, et al. Determination of the purity of pharmaceutical reference materials by 1H NMR using the standardless PULCON methodology. J Pharm Biomed Anal 2014;100:381–6
33. Hoult DI. The principle of reciprocity. J Magn Reson 2011;213:344–6
34. Provencher SW. Estimation of metabolite concentrations from localized in vivo proton NMR spectra. Magn Reson Med 1993;30:672–9
35. Righi V, Roda JM, Paz J, et al. 1H HR-MAS and genomic analysis of human tumor biopsies discriminate between high and low grade astrocytomas. NMR Biomed 2009;22:629–37
36. Jones HC, Lopman BA. The relation between CSF pressure and ventricular dilatation in hydrocephalic HTx rats. Eur J Pediatr Surg 1998; 8(Suppl. 1):55–8
37. Miller JM, McAllister JP. Reduction of astrogliosis and microgliosis by cerebrospinal fluid shunting in experimental hydrocephalus. Cerebrospinal Fluid Res 2007;4:5
38. Eskandari R, Harris CA, McAllister JP. Reactive astrocytosis in feline neonatal hydrocephalus: Acute, chronic, and shunt-induced changes. Childs Nerv Syst 2011;27:2067–76
39. Roales-Bujan R, Paez P, Guerra M, et al. Astrocytes acquire morphological and functional characteristics of ependymal cells following disruption of ependyma in hydrocephalus. Acta Neuropathol 2012;124:531–46
40. Olalla L, Gutierrez A, Campos JA, et al. Nuclear localization of L-type glutaminase in mammalian brain. J Biol Chem 2002;277:38939–44
41. McAllister JP. 2nd. Pathophysiology of congenital and neonatal hydrocephalus. Semin Fetal Neonatal Med 2012;17:285–94
42. Jones HC, Harris NG, Rocca JR, et al. Progressive changes in cortical metabolites at three stages of infantile hydrocephalus studied by in vitro NMR spectroscopy. J Neurotrauma 1997;14:587–602
43. Braun KP, Dijkhuizen RM, de Graaf RA, et al. Cerebral ischemia and white matter edema in experimental hydrocephalus: A combined in vivo MRI and MRS study. Brain Res 1997;757:295–8
44. Kondziella D, Eyjolfsson EM, Saether O, et al. Gray matter metabolism in acute and chronic hydrocephalus. Neuroscience 2009;159:570–7
45. Harris NG, Plant HD, Inglis BA, et al. Neurochemical changes in the cerebral cortex of treated and untreated hydrocephalic rat pups quantified with in vitro 1H-NMR spectroscopy. J Neurochem 1997;68:305–12
46. Braun KP, Vandertop WP, Gooskens RH, et al. NMR spectroscopic evaluation of cerebral metabolism in hydrocephalus: A review. Neurol Res 2000;22:51–64
47. Melø TM, Håberg AK, Risa Ø, et al. Tricarboxylic acid cycle activity measured by 13C magnetic resonance spectroscopy in rats subjected to the kaolin model of obstructed

hydrocephalus. Neurochem Res 2011;36:1801–8
48. Ratai EM, Gilberto Gonzalez R. Clinical magnetic resonance spectroscopy of the central nervous system. Handb Clin Neurol 2016;135: 93–116
49. Miller BL. A review of chemical issues in 1H NMR spectroscopy: N-acetyl-L-aspartate, creatine and choline. NMR Biomed 1991;4:47–52
50. Balestrino M, Lensman M, Parodi M, et al. Role of creatine and phosphocreatine in neuronal protection from anoxic and ischemic damage. Amino Acids 2002;23:221–9
51. Chen G, Wang J. Threonine metabolism and embryonic stem cell self-renewal. Curr Opin Clin Nutr Metab Care 2013;1:80–5
52. Kondziella D, Qu H, Lüdemann W, et al. Astrocyte metabolism is disturbed in the early development of experimental hydrocephalus. J Neurochem 2003;85:274–81
53. Brekke E, Berger HR, Widerøe M, et al. Glucose and intermediary metabolism and astrocyte–neuron interactions following neonatal hypoxia ischemia in rat. Neurochem Res 2017;42:115–32
54. Zhou Y, Danbolt NC. Glutamate as a neurotransmitter in the healthy brain. J Neural Transm 2014;121:799–817
55. Choi D. Glutamate neurotoxicity and diseases of the nervous system. Neuron 1988;1:623–34
56. Spanaki C, Kotzamani D, Petraki Z, et al. Heterogeneous cellular distribution of glutamate dehydrogenase in brain and in non-neural tissues. Neurochem Res 2014;39:500–15
57. McKenna MC, Stridh MH, McNair LF, et al. Glutamate oxidation in astrocytes: Roles of glutamate dehydrogenase and aminotransferases. J Neurosci Res 2016;94:1561–71
58. Erecinska M, Silver IA. Metabolism and role of glutamate in mammalian brain. Prog Neurobiol 1990;35:245–96
59. Chen Y, Swanson RA. Astrocytes and brain injury. J Cereb Blood Flow Metab 2003;23:137–49
60. Danbolt NC, Furness DN, Zhou Y. Neuronal vs glial glutamate uptake: Resolving the conundrum. Neurochem Int 2016;98:29–45
61. Yatomi Y, Tanaka R, Shimura H, et al. Chronic brain ischemia induces the expression of glial glutamate transporter EAAT2 in subcortical white matter. Neuroscience 2013;244:113–21
62. McNatt SA, McComb JG, Nelson MD, et al. Proton magnetic resonance spectroscopy of hydrocephalic infants. Pediatr Neurosurg 2007;43:461–7
63. Dringen R, Brandmann M, Hohnholt MC, et al. Glutathione-dependent detoxification processes in astrocytes. Neurochem Res 2015;40:2570–82
64. Dringen R. Metabolism and functions of glutathione in brain. Prog Neurobiol 2000;62:649–71
65. Moffett JR, Ross B, Arun P, et al. N-Acetylaspartate in the CNS: From neurodiagnostics to neurobiology. Prog Neurobiol 2007;81:89–131
66. Chakraborty G, Mekala P, Yahya D, et al. Intraneuronal N-acetylaspartate supplies acetyl groups for myelin lipid synthesis: Evidence for myelin-associated aspartoacylase. J Neurochem 2001;78:736–45
67. Sacha P, Zamecnık J, Barinka C, et al. Expression of glutamate carboxypeptidase II in human brain. Neuroscience 2007;144:1361–72

68. van der Veen JN, Kennelly JP, Wan S, et al. The critical role of phosphatidylcholine and phosphatidylethanolamine metabolism in health and disease. Biochim Biophys Acta 2017;1859:1558–72
69. Ousley AH, Morell P. Individual molecular species of phosphatidylcholine and phosphatidylethanolamine in myelin turn over at different rates. J Biol Chem 1992;267:10362–9
70. Rao AM, Hatcher JF, Dempsey RJ. Lipid alterations in transient forebrain ischemia: Possible new mechanisms of CDP-choline neuroprotection. J Neurochem 2000;75:2528–35
71. Jackson PS, Strange K. Volume-sensitive anion channels mediate swelling activated inositol and taurine efflux. Am J Physiol 1993;265:C1489–500
72. Strange K, Emma F, Paredes A, et al. Osmoregulatory changes in myoinositol content and Naþ/myo-inositol cotransport in rat cortical astrocytes. Glia 1994;12:35–43
73. Ripps H, Shen W. Review: Taurine: A “very essential” amino acid. Mol Vis 2012;18:2673–86
74. Vitvitsky V, Garg SK, Banerjee R. Taurine biosynthesis by neurons and astrocytes. J Biol Chem 2011;286:32002–10
75. Saransaari P, Oja SS. Taurine and neural cell damage. Amino Acids 2000;19:509–26

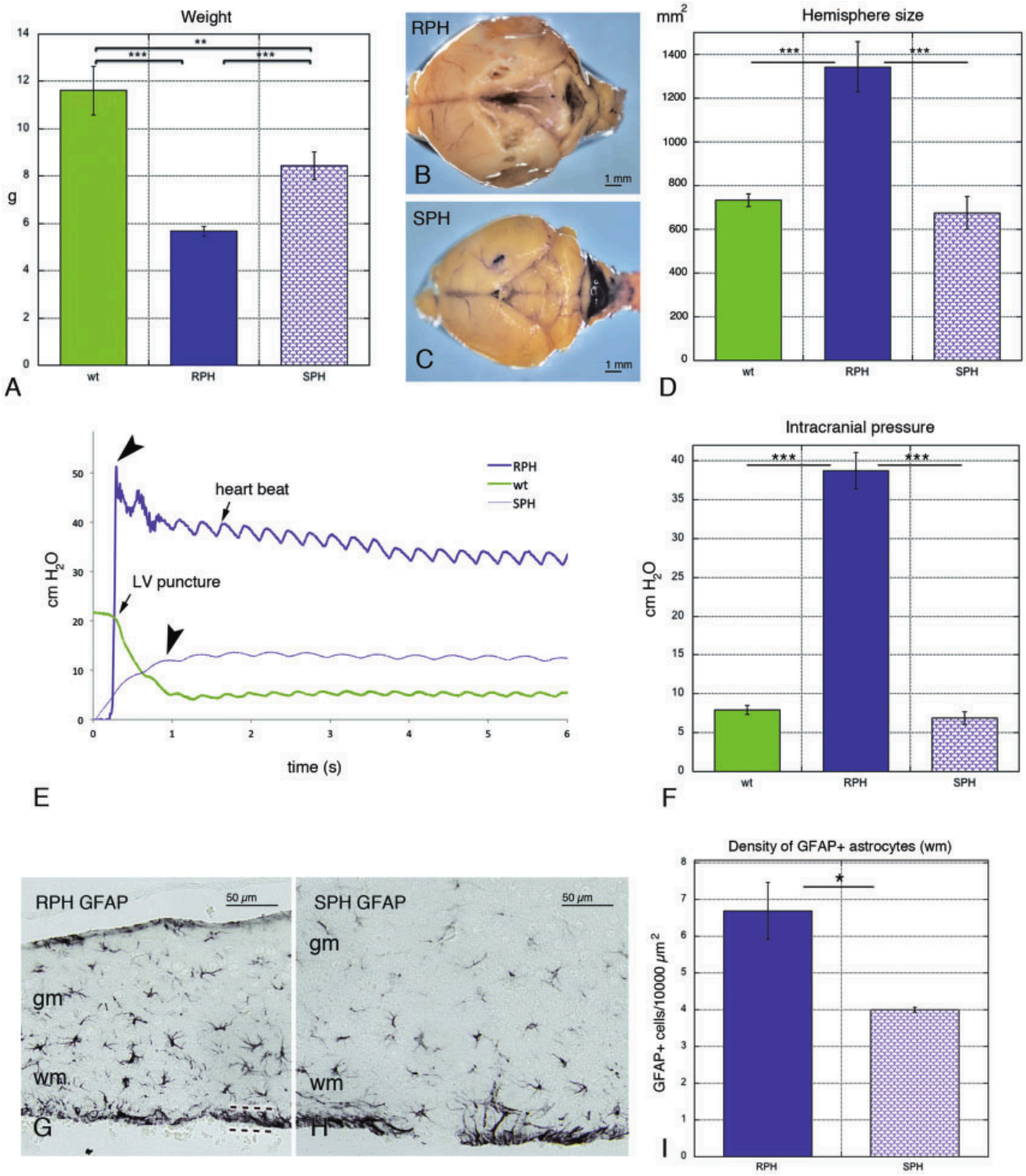

FIGURE 1. Brain size, intracranial pressure (ICP) and astrocytes in normal mice (wild-type, wt) and mice with rapidly (RPH) and slowly (SPH) progressive hydrocephalus. Mice were selected according to the criteria described by Batiz et al (26). (A) Weight of the mice used for the metabolic spectral analysis. (B, C) Dorsal views of the brains from mice with RPH and SPH used for ICP measurement. (D) The hemisphere size of normal mice (wt) and mice with RPH and SPH used for ICP measurement was estimated by multiplying the dorsal and lateral views. (E) Representative time course of ICP in normal

mice (wt, green line), mice with RPH (thick blue line), and mice with SPH (thin blue line). Pressure waves from heart pulsations were detected. (F) Bar graph representation of the ICP from the 3 groups of animals. (G, H) GFAP immunostaining in frontal paraffin sections of hyh mice with rapidly (RPH, G) and slowly (SPH, H) progressive hydrocephalus. GFAP-positive reactive astrocytes formed a cell layer covering ependyma-denuded surfaces (between dashed lines, in G). GFAP-positive astrocytes could also be detected in the periventricular white matter (wm) and in the deep gray matter (gm). (I) Density of GFAP-positive astrocytes (cells/area) in the white matter in the parietal cortex of mice with RPH and SPH. *$p < 0.05$, **$p < 0.005$, ***$p < 0.0001$; Student t-test

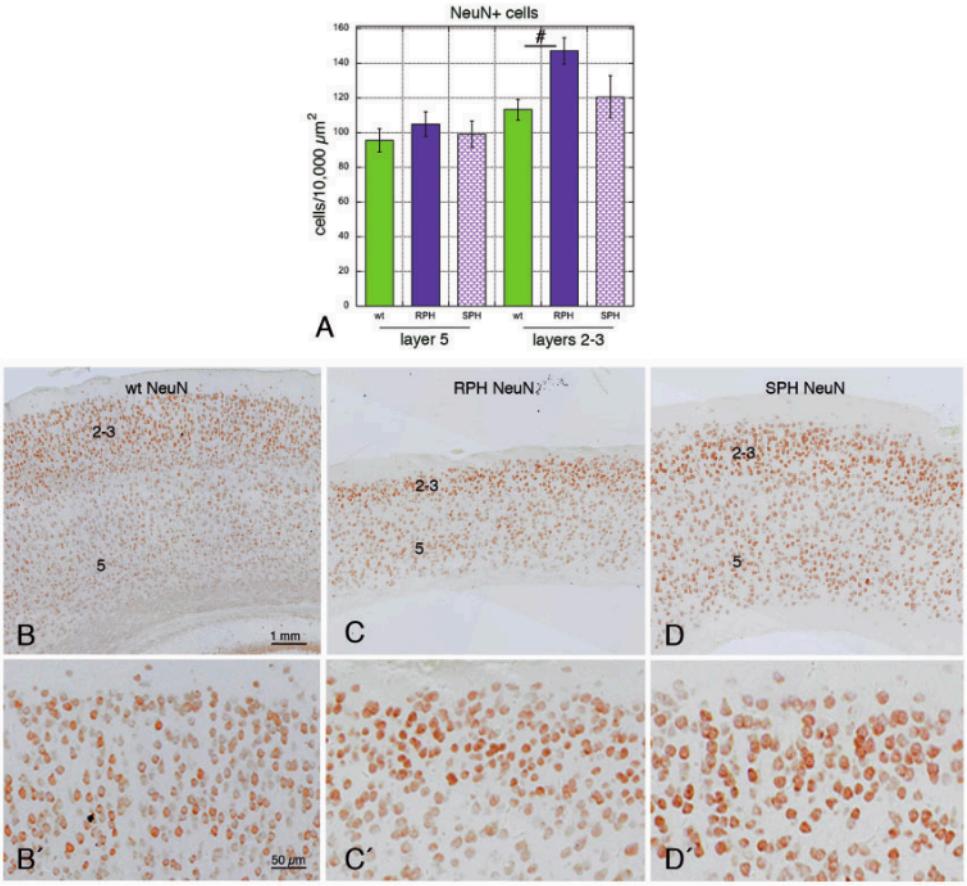

FIGURE 2. Neuronal density (NeuN-positive cells/area) in the parietal cortex of normal mice (wt) and mice with rapidly (RPH) and slowly (SPH) progressive hydrocephalus (A). Data are represented for cortical areas 2–3 and 5. (B–D) NeuN immunostaining in paraffin sections of the parietal cortex of wt mice and hyh mice with RPH and SPH. The cortical layers (2, 3, and 5) used for the quantification shown in (A) are labeled. (B0 –D0) Details of layers 2–3 from the same mice and sections. The magnifications in B–D and B0 –D0 were the same. #p < 0.05; Wilcoxon-Mann-Whitney test.

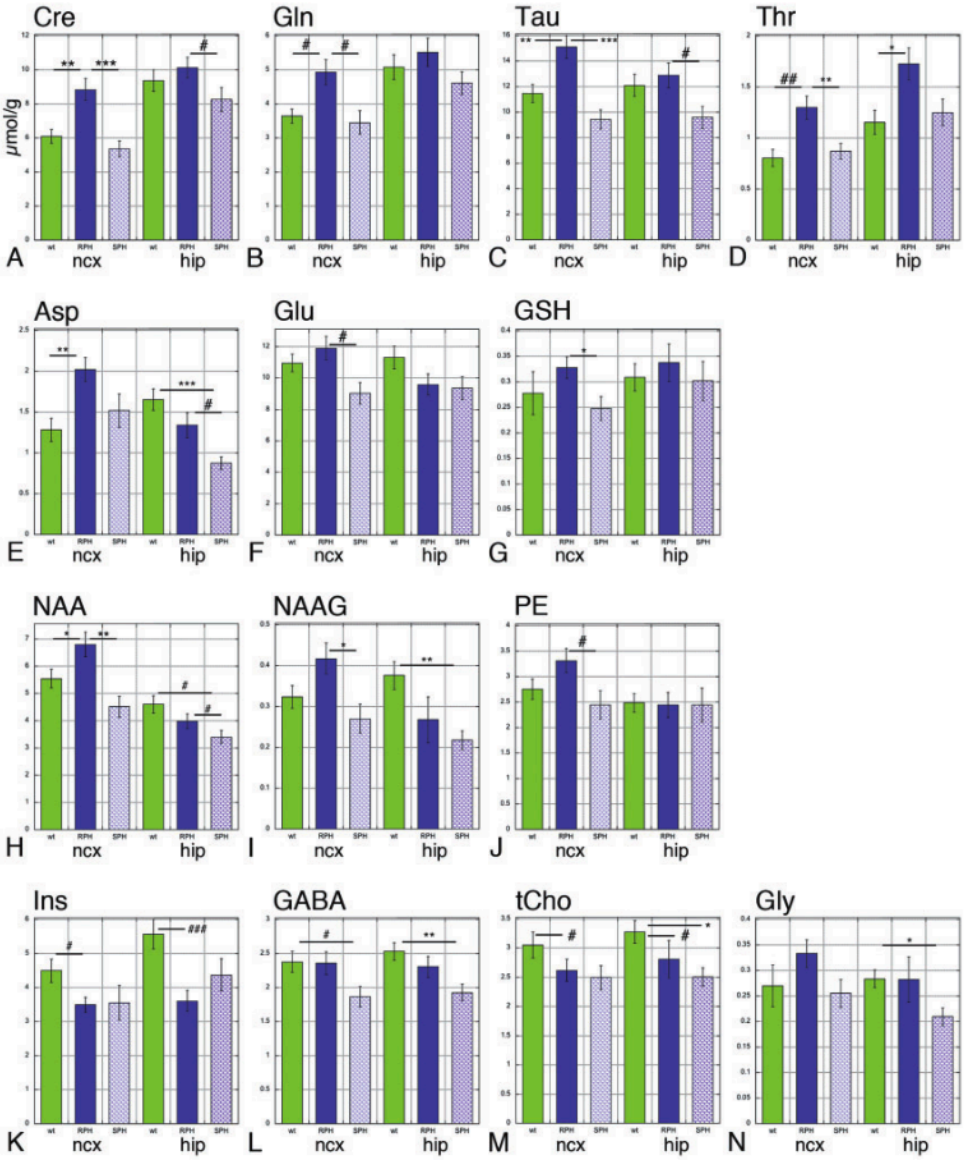

FIGURE 3. Levels of aspartate (Asp, A), glutamine (Gln, B), taurine (Tau, C) threonine (Thr, D), aspartate (Asp, E), glutamate (Glu, F), glutathione (GSH, G), N-acetyl-aspartate (NAA, H), N-acetyl-aspartyl-glutamate (NAAG, I), phosphatidylethanolamine (PE, J), inositol (Ins, K), GABA (L), total choline (tCho, M), and glycine (Gly, N) in the neocortex (ncx) and the hippocampus (hip) of normal (wild-type, wt) mice and animals with rapidly (RPH) and slowly (SPH) progressive hydrocephalus. #$p < 0.05$, ## $p < 0.005$, ###$p < 0.0005$; Wilcoxon-Mann-Whitney test. *$p < 0.05$, **$p < 0.005$, ***$p < 0.0005$; Student t-test.

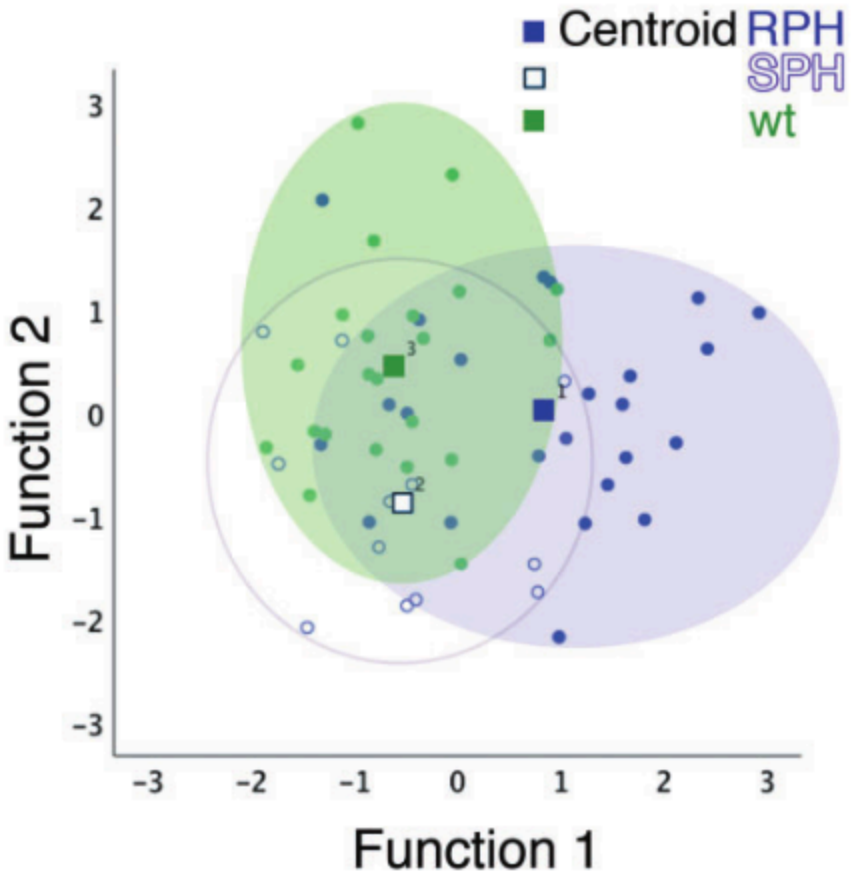

FIGURE 4. Score plot derived from the 1HR-MAS NMR analysis for creatine, N-acetyl-aspartate, taurine, and threonine from biopsies of the neocortex using multivariate analysis. Three groups of mice were used for the analysis: RPH (mice with rapidly progressive hydrocephalus, group 1); SPH (mice with slowly progressive hydrocephalus, group 2); and wt mice (wild-type, group 3). The centroid for each group is shown. Ellipses have been drawn to encompass the majority of samples extracted from the same group. The centroid shows that mice with RPH appear to be clearly separated from the mice with SPH and wt mice.

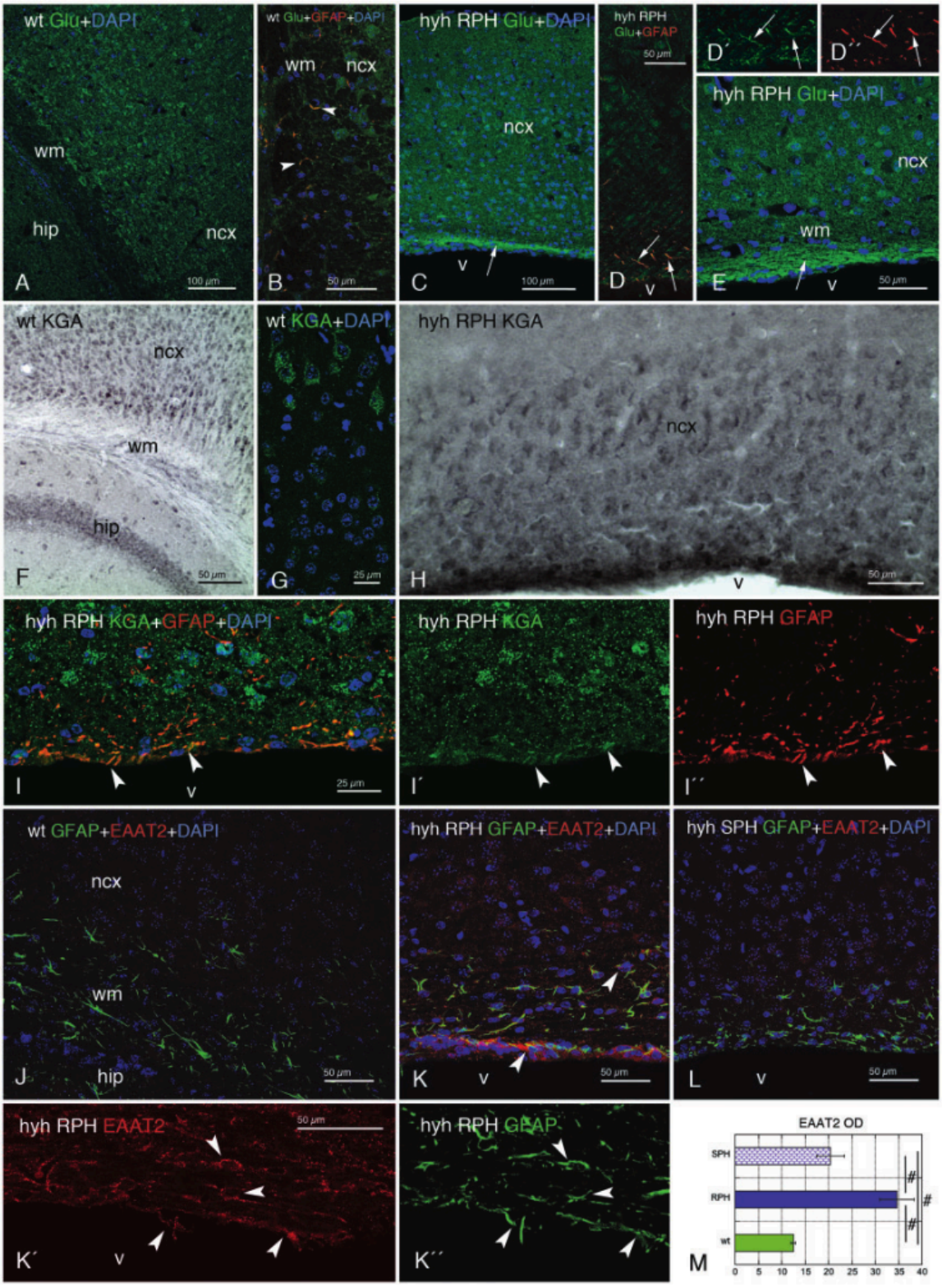
wt Glu+DAPI
wm
hip
ncx
A
100 µm
wt Glu+GFAP+DAPI
wm
ncx
B
50 µm
hyh RPH Glu+DAPI
ncx
v
C
100 µm
hyh RPH Glu+GFAP
50 µm
D
v
D´
D´´
hyh RPH Glu+DAPI
ncx
wm
v
E
50 µm
wt KGA
ncx
wm
hip
F
50 µm
wt KGA+DAPI
G
25 µm
hyh RPH KGA
ncx
v
H
50 µm
hyh RPH KGA+GFAP+DAPI
v
I
25 µm
hyh RPH KGA
I´
hyh RPH GFAP
I´´
wt GFAP+EAAT2+DAPI
ncx
wm
hip
J
50 µm
hyh RPH GFAP+EAAT2+DAPI
v
K
50 µm
hyh SPH GFAP+EAAT2+DAPI
v
L
50 µm
hyh RPH EAAT2
50 µm
K´
v
hyh RPH GFAP
K´´
EAAT2 OD
SPH
RPH
wt
#
#
#
0
5
10
15
20
25
30
35
40
M

FIGURE 5. Immunohistochemistry/immunofluorescence for glutamate, glutaminase, and the excitatory amino acid transporter 2 (EAAT2). Immunolabeling in vibratome sections for glutamate (Glu, fluorescence in green), kidney-type glutaminase (KGA, fluorescence in green and DAB-nickel reaction), and GFAP (fluorescence in red) in the neocortex (ncx) of normal mice (wt; A, B, F, G) and hyh mice with rapidly progressive hydrocephalus (RPH; C–E, H, I). (D0 /I0) and (D00 /I00) correspond to the green and red channels for immunofluorescence of (D/I) to show colocalizations (arrowheads). A confocal plane (1 mm-thick) is shown in (D). Nuclear staining in blue with DAPI. Arrowheads in (B) point to astrocytes immunolabeled for GFAP and glutamate in the gray matter and white matter (wm) of the neocortex. Arrows in (C–E) point to the periventricular astrocyte reaction in the white matter. Abbreviations: hip, hippocampus. Immunofluorescence in frozen sections (confocal planes 1 mm thick) for EAAT2 (fluorescence in red) and GFAP (fluorescence in green) in the 3 groups of mice: normal (J) and with rapidly (K) and slowly (L) progressive hydrocephalus. Immunolabeling was detected in astrocytes (arrowheads; K). (K0) and (K00) correspond to the red and green channels for immunofluorescence of (K) to show colocalizations. Mean optical density (OD) for EAAT2 immunofluorescence in wt mice and mice with RPH and SPH. #$p < 0.05$ Wilcoxon-Mann-Whitney test. Abbreviations: hip, hippocampus; v, lateral ventricle lumen.

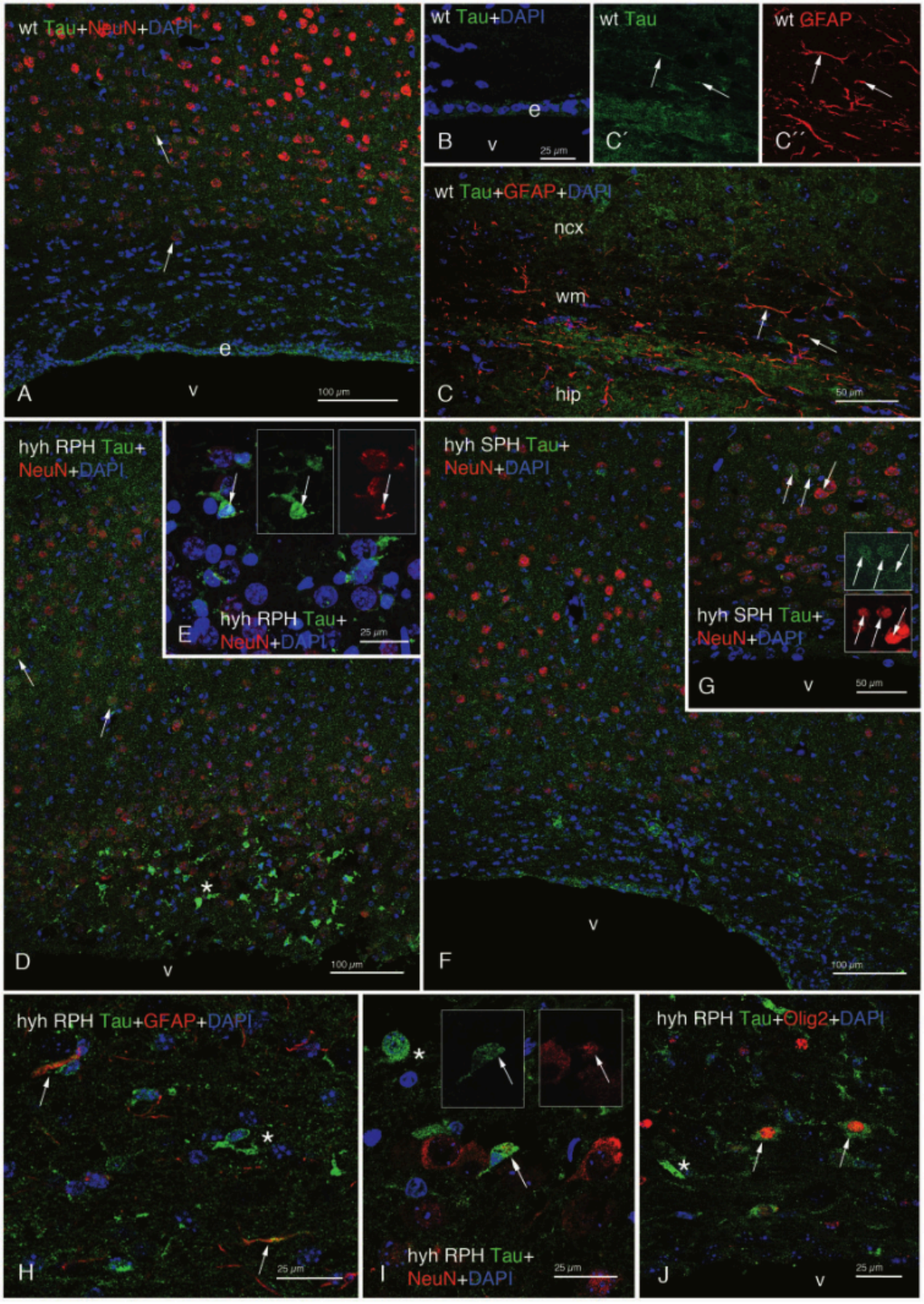
wt Tau+NeuN+DAPI
e
A
v
100 µm
wt Tau+DAPI
e
B
v
25 µm
wt Tau
C´
wt GFAP
C´´
wt Tau+GFAP+DAPI
ncx
wm
hip
C
50 µm
hyh RPH Tau+
NeuN+DAPI
E
hyh RPH Tau+
NeuN+DAPI
25 µm
*
D
v
100 µm
hyh SPH Tau+
NeuN+DAPI
hyh SPH Tau+
NeuN+DAPI
G
v
50 µm
v
F
100 µm
hyh RPH Tau+GFAP+DAPI
*
H
25 µm
*
hyh RPH Tau+
NeuN+DAPI
I
25 µm
hyh RPH Tau+Olig2+DAPI
*
J
v
25 µm

FIGURE 6. Immunofluorescence in vibratome sections for taurine (Tau; fluorescence in green), GFAP (fluorescence in red), NeuN (nuclear neuron marker; fluorescence in red), and Olig2 (oligodendrocyte marker; fluorescence in red) in the neocortex of normal mice (wt; A–C) and hyh mice exhibiting rapidly progressive hydrocephalus (RPH; D, E, H–J) and slowly progressive hydrocephalus (SPH; F, G). Nuclear staining in blue with DAPI. Taurine immunolabeling is present in astrocytes (arrows; C, H), neurons (arrows; D, G), and ependymocytes (e; A, B) of wt and hyh mice. Strong taurine immunolabeling of periventricular cells (asterisk; E), including neurons (arrows; E, I) and oligodendrocytes (arrows; J), was observed in mice with RPH. Inserts in E, G, and I correspond to channels for red and green fluorescence. Abbreviations: hip, Hippocampus; ncx; neocortex; v, laterl ventricle lumen; wm, withe matter.